

ORGANIC-INORGANIC GRAPHITE AND TRANSITION METAL
DICHALCOGENIDES BASED COMPOSITES FOR 3D PRINTING

JORGE ALFREDO CATALAN GONZALEZ

MASTER'S PROGRAM IN METALLURGICAL AND MATERIALS ENGINEERING

APPROVED:

Anupama B. Kaul, Ph.D., Chair

Stephen Stafford, Ph.D.

Shailendra K. Varma, Ph.D.

Charles Ambler, Ph.D.
Dean of the Graduate School

Copyright ©

by

Jorge Alfredo Catalan Gonzalez

2017

PREVIEW

Dedication

I would like to dedicate this work to my mother, father, brother, cousins, and friends. Also, I would like to make a special mention and dedication to my uncle Fernando González, who passed the way 9 years ago. While he was alive, he was to me: a father, a friend and a teacher... simply the best human being I have met.

PREVIEW

PREVIEW

ORGANIC-INORGANIC GRAPHITE AND TRANSITION METAL
DICHALCOGENIDE BASED COMPOSITES FOR 3D PRINTING

by

JORGE ALFREDO CATALAN GONZALEZ, M.S. MME

THESIS

Presented to the Faculty of the Graduate School of

The University of Texas at El Paso

in Partial Fulfillment

of the Requirements

for the Degree of

MASTER OF SCIENCE

METALLURGICAL, MATERIALS AND BIOMEDICAL ENGINEERING

THE UNIVERSITY OF TEXAS AT EL PASO

December 2017

ProQuest Number: 10688449

All rights reserved

INFORMATION TO ALL USERS

The quality of this reproduction is dependent upon the quality of the copy submitted.

In the unlikely event that the author did not send a complete manuscript and there are missing pages, these will be noted. Also, if material had to be removed, a note will indicate the deletion.



ProQuest 10688449

Published by ProQuest LLC (2018). Copyright of the Dissertation is held by the Author.

All rights reserved.

This work is protected against unauthorized copying under Title 17, United States Code
Microform Edition © ProQuest LLC.

ProQuest LLC.
789 East Eisenhower Parkway
P.O. Box 1346
Ann Arbor, MI 48106 – 1346

Acknowledgements

I wish to specially thank my professor and advisor Dr. Anupama B. Kaul, for being an excellent and patient mentor. Without her excellent mentoring skills and sponsoring a Research Assistant position for me, I would not be able to grow as a graduate student. I will never forget that she helped me to give my first oral presentation at the American Vacuum Society (AVS) international conference held in Nashville, Tennessee in November 2016. This was one of the most fulfilling experiences that I have had in my career. Also, under her guidance I was able to learn a great deal about two-dimensional (2D) materials, a topic that is of much scientific interest. I do not have words to describe how grateful I feel for having this opportunity to work in Dr. Kaul's research group.

Moreover, I wish to thank Dr. Stephen Stafford and Dr. Shailendra Varma for accepting to be on my thesis committee. It is a great honor for me to have two of the best Professors in the Metallurgy, Materials and Biomedical Engineering department as graduate mentors. Also, I would like to thank Professor Witold Brostow and his students, Nathalie Hnatchuk and I Kang Chen from the University of North Texas who helped with some of the mechanical properties measurements that are discussed in this thesis. They graciously agreed to help with obtaining some of the mechanical property data on our 3D printed composites from UTEP.

Special thanks also goes to Damaris Cortés and Perla Pérez, summer students from the Army Research Apprentice Program provided to the Kaul Group in Summer 2017, for their help during the extrusion and 3D printing process. They helped a great deal throughout the summer which helped accelerate the work. This was a personally enriching experience for me, since it was my first time working as a mentor for two junior students. Also, thanks to Gustavo Saenz, Avra Bandyopadhyay, Ph.D. students in Prof. Kaul's group, for their guidance and useful discussions that has helped improve the quality of this work. Last but not least, I would like to thank Adriana Ramirez, for her help in the set up of the 3D printing instrumentation, as well as the useful tips she provided during the extrusion and 3D printing process.

Abstract

This project was multipronged to help fuse together topics of additive manufacturing and two-dimensional (2D) layered materials, and studying the mechanical and electrical properties of the composites produced. The composites are made from the thermoplastic polymer acting as a matrix and the graphite and 2D transition metal dichalcogenides (TMDs) serving as the filler or reinforcement. Different concentrations of TMD's were added to the matrix to study the effect of composition on the mechanical and electrical properties. To shed insights into the mechanical properties, test coupons were produced as “dog bone” structures for tensile testing using the ASTM D638 type 5 standard, which were printed with the aid of a Lulzbot TAZ 6 3D printer. In the same way, two-terminal resistor-like structures were printed to test the electrical properties inherent to the composites.

From the measurements conducted, polyethylene terephthalate glycol (PETG) – graphite composites had a yield strength (YS) ≈ 50 MPa, an ultimate tensile strength (UTS) ≈ 30 MPa and had a better ductility (strain to rupture $\approx 8\%$) compared to the acrylonitrile butadiene styrene (ABS) composite counterparts. Also, molybdenum disulfide (MoS_2) had a more positive effect than tungsten disulfide (WS_2), since the strength was retained while the ductility was increased at low loadings of the material. Strain levels were measured to be 30% - 120% when adding 1 wt% of MoS_2 and WS_2 . On the other hand, with high additions of MoS_2 and WS_2 (15 and 20 wt%) ductility was completely lost since no plastic deformation occurred during the testing. Moreover, PETG – graphite resistor-like structures were 3-dimensional (3D) printed and tested with the help of a semiconductor parameter analyzer. All samples were tested at different radius of curvatures (0 cm^{-1} , 0.072 cm^{-1} , 0.087 cm^{-1} , 0.112 cm^{-1} , 0.157 cm^{-1} , and 0.262 cm^{-1}) which showed a composite that was strain insensitive. The obtained average conductivity and resistivity were $\approx 5.27\text{ Siemens-m}^{-1}$ and 0.250 Ohm-m , respectively. In the process of forming the composites, some pretreatment of the 2D material may also be necessary. We studied one aspect of this pretreatment by looking at particle size measured using dynamic light scattering. The fragmentation rate (FR) of 2D MoS_2 ,

WS₂, and graphite in N-methyl-pyrrolidinone (NMP) was computed in chemical exfoliants, where FR is a measure of the particle size reduction as a function of ultrasonication time. For the 2D layered materials, the highest FR generally occurred for sonication times $t_{sonic} = 30$ min., after which point FR varied less sensitively with t_{sonic} . The highest FR occurred for graphite, where $FR_{Graphite}$ was $\sim -1176.4 \mu\text{m}\cdot\text{hr}^{-1}$, while FR_{WS_2} and FR_{MoS_2} was measured to be $\sim -32.4 \mu\text{m}\cdot\text{hr}^{-1}$ and $\sim -3.8 \mu\text{m}\cdot\text{hr}^{-1}$, respectively. This pretreatment maybe an important step to further tune the properties of the hybrid organic-inorganic composites of 2D materials with polymeric systems for a number of application platforms.

PREVIEW

Table of Contents

Acknowledgements.....	v
Abstract.....	vi
Table of Contents.....	viii
List of Tables	x
List of Figures.....	xi
Chapter 1: Background Information	1
1.1 - Graphene.....	2
1.2 – Transition Metal Dichalcogenides (TMD's).....	4
1.3 – Additive Manufacturing (AM).....	4
1.3.1 Stereolithography (SLA).....	5
1.3.2 Laminated Object Manufacturing (LOM)	6
1.3.3 Selective Laser Sintering (SLS).....	7
1.3.4 Fuse Deposition Modeling (FDM).....	8
1.4 – Composite Materials	10
Chapter 2: Sample Preparation	12
2.1 – Material selection.....	12
2.1.1 Polyethylene terephthalate glycol (PETG)	12
2.1.2 Acrylonitrile butadiene styrene (ABS)	12
2.1.3 Reinforcements	13
2.2 – Filament Extrusion.....	13
2.3 - Printing	19
2.3.1 Tensile test sample printing	19
2.3.2 Resistor design for electrical characterization	23
Chapter 3: Mechanical Properties	25
3.1 – Results.....	26
3.2 – Discussion	45
Chapter 4: Electrical Properties	48
4.1 – Results.....	48
4.1.1 Step Annealing versus Continuous Annealing	49

4.1.2 Substrate vs No Substrate Analysis	55
4.1.3 I-V Measurements 1 st Resistor Design.....	59
4.1.4 Application in Wearable Electronics	62
4.2 – Discussion	65
Chapter 5: Particle Size Analysis.....	68
5.1 – Molybdenum Disulfide (MoS ₂)	68
5.2 – Tungsten Disulfide (WS ₂).....	71
5.3 – Graphite.....	73
5.4 – Discussion	75
Chapter 6: Conclusions and Future Work.....	76
References	78
Appendix: Procedure for 3D Printing	83
Vita	85

List of Tables

Table 1: Lulzbot TAZ 6 Printing Parameters.	22
--	----

PREVIEW

List of Figures

Figure 1.1 Two different stereolithography schematics. a) Bath stereolithography consists of a laser curing a layer of liquid resin. After on layer is cured, the stage lowers itself allowing for more liquid resin to cover the cured polymer. After that, laser cures the new layer of resin as specified by the design. b) This approach works in reverse process compared to the bath SLA. Here the sage is submerged inside the resin. Then, the stage is pulled up to allow more resin to flow below the cured polymer. A patter can be added so that the laser can cured the whole layer design at the same time. Obtained from Ref[37]	5
Figure 1.2 Schematic of Laminated Object Manufacturing (LOM) process. Obtained from Ref [36]......	6
Figure 1.3 Schematic of selective laser sintering (SLS) process. Obtained from Ref [36].	8
Figure 1.4 Schematic of fused deposition modeling (FDM) process. Obtained from Ref[36]....	9
Figure 2.1 Side view of Filabot EX2 extruding system.	14
Figure 2.2 Filabot spooling system. It is placed in front of the extruder to create spools of the extrude filament. Also, it helps to regulate the filament size.....	15
Figure 2.3 Silverson L5M-A Laboratory Shear.	15
Figure 2.4 Schematic of the hand mixing process to produce uniform mixtures of solid compounds. This process is similar to the one made by a cement truck mixer.	17
Figure 2.5 Filament coming out of the Filabot extruder. The 90° angle created by the filament allows the user to know that the extrusion and spooling speed are synchronized. Having this synchronization is crucial in obtaining a certain filament diameter. If the filament is extruding faster than what the spooling can handle, then the filament will be thick (big diameter) and most likely it will knot itself up. On the other hand, if the extrusion speed is to slow and spooling	

speed is faster, the filament diameter will be too thin due to the excessive pulling force produced by the spooler.	18
Figure 2.6 (a) Frontal view of tensile specimen ASTM D638 type 5. (b) Isometric view of the “dog bone” sample.	20
Figure 2.7 Two different resistor like structures. Left structure (with complicated geometry) has higher resistance due to the overall longer channel length. Right structure is simple but allows faster designs and is easier to handle during electrical characterization.	24
Figure 2.8 Small, medium, and large resistor like structures for electrical characterization.	24
Figure 3.1 (a) & (b) Stress vs strain plots of ABS and ABS – 1wt% graphite. Each graph shows 10 different measurements. Each measurement corresponds to 1 “dog bone” sample.	27
Figure 3.2 (a) & (b) Stress vs strain plots of ABS – 5wt% and ABS – 10wt% graphite. Each graph shows 10 different measurements. Each measurement corresponds to 1 “dog bone” sample.	28
Figure 3.3 (a) & (b) Stress vs strain plots of ABS – 15wt% and ABS – 20wt% graphite, respectively. Each graph shows 10 different measurements. Each measurement corresponds to 1 “dog bone” sample.	29
Figure 3.4 (a) & (b) Stress vs strain plots of PETG and PETG – 1wt% graphite. Each graph shows 10 different measurements. Each measurement corresponds to 1 “dog bone” sample. ...	31
Figure 3.5 (a) & (b) Stress vs strain plots of PETG – 5wt% and PETG – 10wt% graphite, respectively. Each graph shows 10 different measurements. Each measurement corresponds to 1 “dog bone” sample.	32

Figure 3.6 (a) & (b) Stress vs strain plots of PETG – 15wt% and PETG – 20wt% graphite, respectively. Each graph shows 10 different measurements. Each measurement corresponds to 1 “dog bone” sample.....	33
Figure 3.7 (a) & (b) Stress vs strain plots of PETG and PETG – 1wt% MoS ₂ . Each graph shows 10 different measurements. Each measurement corresponds to 1 “dog bone” sample.	35
Figure 3.8 (a) & (b) Stress vs strain plots of PETG – 5wt% and PETG – 10wt% MoS ₂ , respectively. Each graph shows 10 different measurements. Each measurement corresponds to 1 “dog bone” sample.....	36
Figure 3.9 (a) & (b) Stress vs strain plots of PETG – 15wt% and PETG – 20wt% MoS ₂ , respectively. Each graph shows 10 different measurements. Each measurement corresponds to 1 “dog bone” sample.....	37
Figure 3.10 (a) & (b) Stress vs strain plots of PETG and PETG – 1wt% WS ₂ . Each graph shows 10 different measurements. Each measurement corresponds to 1 “dog bone” sample.	39
Figure 3.11 (a) & (b) Stress vs strain plots of PETG – 5wt% and PETG – 10wt% WS ₂ , respectively. Each graph shows 10 different measurements. Each measurement corresponds to 1 “dog bone” sample.....	40
Figure 3.12 (a) & (b) Stress vs strain plots of PETG – 15wt% and PETG – 20wt% WS ₂ , respectively. Each graph shows 10 different measurements. Each measurement corresponds to 1 “dog bone” sample.....	41
Figure 3.13 Comparison between ABS (a) and PETG (b) stress vs strain curves with graphite. (a) ABS series show a series of lines corresponding to control, 1 wt%, 5 wt%, 10 wt%, 15 wt%, and 20 wt%. (b) PETG – graphite series lines correspond to the same loadings as in (a).....	42

Figure 3.14 (a) Young's modulus of each ABS polymer composite with different graphite loadings. (b) Strain at failure for each ABS – graphite composite.	43
Figure 3.15 (a) Young's modulus (YM) of each PETG polymer composite with different graphite loadings. (b) Strain at failure for each PETG – graphite composite.....	43
Figure 3.16 Comparison between PETG MoS ₂ (a) and WS ₂ (b) stress vs strain curves. (a) MoS ₂ series show a series of lines corresponding to control, 1 wt%, 5 wt%, 10 wt%, 15 wt%, and 20 wt%. (b) WS ₂ series lines correspond to the same loadings as in (a).	44
Figure 3.17 (a) Young's modulus (YM) of each PETG polymer composite with different MoS ₂ loadings. (b) Strain at failure for each PETG – MoS ₂ composite.....	44
Figure 3.18 (a) Young's modulus (YM) of each PETG polymer composite with different WS ₂ loadings. (b) Strain at failure for each PETG – WS ₂ composite.....	45
Figure 3.19 (a) SEM picture of as received graphite powder. Average particle size of about 600 μm. (b) Graphite powder after 4 hours of shear mixing at 6000 rpm. Particle size decreased to average size of around 5 μm.	47
Figure 3.20 Particle size comparison. (a) As received graphite powder particles. (b) As received MoS ₂ powder particle size. (c) WS ₂ as received particles. Graphite particle size was the biggest of all three 2D materials. Further treatment to reduce the particle size was needed to prevent 3D printer's nozzle clogging and at the same time improved matrix – filler uniformity.	47
Figure 4.1 Micromanipulator and semiconductor parameter analyzer (HP 4156A) set up used to measure electrical properties of the conductive printed structures.	49
Figure 4.2 Step Annealing of the 3 sets of samples formed by small, medium and large. (a) – (c) Shows data regarding current levels at 20V every 1 hour. Blue, red, and green represent the color small, medium, and large samples, respectively.....	51

Figure 4.3 (a) – (c) I-V curves of not annealed small, medium, and large resistor like structures.	52
Figure 4.4 (a) – (b) Correspond to the I-V curves of small, medium, and large annealed for 4 hours at 80 °C resistor samples, respectively.	53
Figure 4.5 (a) –(b) Show the Current vs Radius of curvature plots. The three plots contain blue lines (not annealed samples data) and red lines (annealed samples data). From top to bottom (a) correspond to small size structures, (b) to medium size, and (c) to large size.	54
Figure 4.6 All five bending structures, with their corresponding radius of curvature values, designed to test the flexibility and sensitivity of printed structures.	55
Figure 4.7 Two set of three 50 wt% graphite – PETG samples. The first set on the left is composed of three samples (small, medium and large). These three samples were not printed on any surface. On the other hand, the set on the right was printed on top of PET substrate.	56
Figure 4.8 (a) – (c) Correspond to small, medium, and large specimens that were not printed on any type of surface. All samples were tested electrically tested using 5 different bending structures (shown in Figure 4.6). No sensitivity to the bending is detected like in a, however there are some graphs ((b) & (c)) showing son discrepancies. These discrepancies are due to contact issues between the probes and the surface of the samples.	57
Figure 4.9 (a) – (c) I-V curves of samples (small, medium, and large) printed on PET substrate. All samples were tested electrically tested using 5 different bending structures (shown in Figure 4.6).	58
Figure 4.10 This graph represents the current values at 20 V of small, medium, and large samples from both sets (with no substrate and with PET substrate). Dotted/dashed lines represent data taken from samples printed on top of the PET substrate, while continuous lines are	

used to represent data from no substrate samples. The minimum current value was around 5 mA, while the highest was about 23 mA. 59

Figure 4.11 (a) – (e) I-V graphs with corresponding picture. Each picture is marked with a red line. Extreme ends of red line on each picture represent the place where probes were placed in order to take electrical data. The channel length increases from top to bottom (red line is longer). As channel length increases, current level decreases..... 61

Figure 4.12 Current values at 20 V for different channel lengths. All lines are almost a straight line, meaning no sensitivity to the radius of curvature. 62

Figure 4.13 Data gather from a medium size resistor structure mounted on an index finger. (a) – (d) Shows the different finger positions during these measurements. (e) I-V graph of all 4 different finger positions. All lines overlap because resistor like structure is not sensitive to the different movements showed in the pictures. 64

Figure 5.1 (a) Particle size distribution measured using the MicroTac for $t_{\text{sonic}} = 0$ min. (control), 30 min., 6 hr, 12 hr and 18 hr.; inset shows the peaks in the MoS_2 distribution at lower length scales. (b) Mean particle size S as a function of t_{sonic} showing the 1st, 2nd and 3rd modes in the distribution function. (c) SEM micrographs showing a higher population of smaller particles in the background for samples where $t_{\text{sonic}} = 18$ hr (iii) compared to the control (i). (d) Raman Spectra..... 70

Figure 5.2 Characterization of treated WS_2 in (a) - (d). (a) Particle size distribution showing $S_{\text{WS}_2} \sim 18.5 \text{ } \mu\text{m}$ for as received material and the inset shows the WS_2 particles over smaller length scales. (b) S as a function of t_{sonic} showing the 2nd mode occurring at $t_{\text{sonic}} = 12$ hr. (c) WS_2 SEM micrographs showing a higher population of smaller particles in the background for the longer $t_{\text{sonic}} = 18$ hr in (iii) compared to the control (i). (d) Raman Spectra. 72

Figure 5.3 (a) Particle size distribution measured using the MicroTac for graphite; inset shows the peaks in the graphene distribution at lower length scales. (b) S as a function of t_{sonic} showing the 1st and 2nd modes in the distribution. (c) SEM micrographs showing a higher population of smaller particles in the background for the longer $t_{\text{sonic}} = 18$ hr in (iii) compared to the control in (i). (d) Raman spectra. 74

PREVIEW

Chapter 1: Background Information

Two-dimensional layered materials have gained increased popularity since the discovery of graphene in 2004 by Geim and Novoselov.^[1] Before 2004, through thermodynamic considerations it was believed that single atom layers of any material would not stable,^[2] but this notion was later denounced after these two renowned scientists isolated a single layer of carbon atoms, called graphene on a Silicon substrate. In order to achieve this, they implemented what it is known as the “scotch tape” technique. In this method, a flake of graphite was placed on scotch tape, and then multiple layers were peeled off from the graphite flake, until one single layer of carbon atoms remained glued to the scotch tape. Once transferred onto an oxidized silicon substrate, this layer of material showed remarkable electrical, thermal, mechanical, and optical properties,^[2,3] opening a new door that promised to revolutionize the technology in our electronic devices, to potentially replace silicon. While graphene has played a pivotal role in the 2D layered materials field, it however does not possess an inherent bandgap. Due to the lack of a band gap, scientists worked on trying to induce a band gap in graphene; alternatively, they also considered looking at different materials that showed a similar structure to graphene. The materials that simulated this honeycomb-like structure of graphene happened to be the transition metal dichalcogenides, materials that have been used since the 1960's^[4] as dry lubricants.

In the same way, additive manufacturing increased its popularity after 2009, when patents regarding this technology expired. Due to these two recent episodes, researchers started to develop new materials that could retain some of the 2D materials' properties and to be processed and manufactured using one of the existing additive manufacturing technologies. Polymer composite materials were the selection of choice, since thermoplastic could act as the matrix of the composite, since their relative low melting and low glass transition temperatures make them suitable to be 3D printed using a method known as, fused deposition modeling (FDM). Also, these polymer matrices were already used along with carbon fibers. So, the exchange of carbon fibers with graphite, graphene, and or any other TMD particles, seemed a plausible option to act as the reinforcement

agent in these polymer based composites. In order to have a better understanding of these topics, I will provide background on: graphene, TMDs, additive manufacturing techniques, and composite materials.

1.1 - Graphene

As mentioned above graphene is considered an allotrope of carbon that was first discovered at Manchester University by Geim and Novoselov in 2004. Graphene is said to be the building block for other carbon allotropes since it is a single layer of sp^2 hybridized carbon atoms. If this layer is taken and then rolled as tubes we will end up with what is known as a single-walled carbon nanotube. In the same way, if it is wrapped around like a sphere we will end up with fullerenes (bucky balls). Lastly, if the single layers are re-stacked again, graphite will be the final outcome. Before this, it was believed that under ambient conditions, single layer materials were not stable enough to remain as a solid. Impressively, graphene showed to the world that a single sheet of carbon atoms could exist without the need of a substrate. Usually, substrates provide enough stability for single layer materials to exist. This led to fascinating studies of graphene, exposing impressive thermal, optical, electrical and mechanical properties for various applications such as: strain sensors, health monitoring sensors, transparent screens, flexible electronics, gas filtering systems, and photovoltaics, among others.^[5-12] Unfortunately, graphene carries its own problems that keep the research community scratching the back of their heads trying to find possible solutions. First, commercial production of graphene is still not possible since most techniques that allow a high yield, high quality and large area are very expensive to be economically efficient for companies. The most important problem with graphene is its lack of a band gap because it limits the possible applications of the material. This is a serious problem specially in electronic devices since it was believed that graphene was going to replace silicon, originating a new era of faster and smaller electronic devices, but because it does not have a band gap this is still not possible.

There are different approaches that scientists have come out with in order to produce high quality, and high yields of graphene. These approaches can be separated into two main topics: top-down approach and bottom-up approach. Top-down approaches, as the names implies, generally consist of starting up with a bulk material (in this case graphite), and then start reducing the number of layers until a single layer is achieved. This top-down approach can be divided into two common sub-categories: mechanical exfoliation^[13-16] and chemical exfoliation.^[17-20] Mechanical exfoliation uses external agents such as scotch tape or solvents to peel off or break off the stacks of bulk material. In fact, “scotch tape” method was the one used in the discovery of graphene. Solvent-based exfoliation techniques^[21-25] are gaining more popularity since they have a high yield of graphene flakes at the expense of size. In this technique, a solvent such as N-methyl-2-pyrrolidone (NMP) is used and with the help of a bath sonicator, horn tip sonicator, and/or shear mixer, energy is transferred so that tactoids of the materials are broken up in to smaller thinner stacks until single layers are completely separated from each other. On the other hand, chemical exfoliation utilizes the help of ions, especially lithium (Li) ions since they are small enough to fill the space between layers of graphene, and with the help of an electric field single layers of carbon are produced.

The other approach is the “bottom-up” approach,^[26-30] and as as the name implies, here we start by forming a single layer of material and keep depositing subsequent layers until the desired thickness is reached. Bottom-up approaches can be divided into epitaxial growth, physical vapor deposition, and chemical vapor deposition. Epitaxial growth consists on the growth of a single layer of carbon on top of a single crystal of silicon carbide. Physical vapor deposition technique consists of the material in use goes to a vapor state and then it is condensed back, until a layer is deposited on top of a substrate. Lastly, in chemical vapor deposition precursor materials are needed, then they are placed inside a heated vacuum chamber, allowing the reaction of this precursor to be deposited on a substrate placed inside the same chamber. Usually, these methods produce high quality single layers, but they are very expensive.

1.2 – Transition Metal Dichalcogenides (TMD's)

In order to solve problems related to graphene, some researchers try to look for materials that have a similar structure to carbon allotrope. The materials of choice are called transition metal dichalcogenides, which were used in industry as dry lubricants. TMD's are compounds formed by a transition metal from IV B, V B, or VI B families, and a chalcogen (sulfur, selenium, tellurium). This type of compounds has a honeycomb like structure, where the transition metal (molybdenum, tungsten, niobium, etc) is sandwich in between layers of the chalcogen. Metals are covalently bonded to the chalcogen, while Van der Waal forces weakly bond the layers. Due to these weak interlayer bonding, TMDs can be exfoliated into single layers. One interesting feature of TMDs, is that as the number of layers is decrease their band gap changes from indirect to direct type (for most of them). This characteristic makes them suitable to build transistors, emitters and detectors.^[31-34] In fact, some of the most common TMDs are: molybdenum disulfide (MoS_2), tungsten diselenide (WSe_2), and tungsten disulfide (WS_2).

1.3 – Additive Manufacturing (AM)

Additive Manufacturing^[18-20, 35-37] can be defined as the process of joining layers of materials until the desired shape and size of a product is achieved. AM is a term, that although interchangeable, exists since the 1980's. This process gained the attention of the research community because it initially acted as rapid prototyping tool. This means, that scientists were able to provide a sample of what an object or desired part was going to look like. After some years, different technologies of AM started to appear offering the capability of utilizing different materials such as: metals, ceramics, composites, polymers, and organic materials. With further advances, AM changed from a prototyping idea to an actual manufacturing process, since AM allowed to design and process objects with complicated geometries in a small period of time. Moreover, it did not produce nearly as much waste material as a conventional top-down manufacturing approach. In fact, AM keeps growing specially in the aerospace industry since the different available technologies allowed to 3D print components composed of complicated metals,

alloys and super alloys, that by conventional casting and machining methods hard to produce due to their hardness and machinability. Lastly, some of the most common AM technologies are: Stereolithography (SLA), Laminated Object Manufacturing (LOM), Selective Laser Sintering (SLS), and Fused Deposition Modeling (FDM).

1.3.1 Stereolithography (SLA)

This AM technology takes advantage of the photosensitivity concept. The way it works is that a photosensitive polymer resin is selected as the printable material. This material is fed in to a container that with the help of rollers or some other type of components will uniformly spread the photosensitive material across a surface. Then, the computer will help a laser to trace the first layer shape on top of the liquid photosensitive resin. When in contact with the laser, the sensitive to light resin will undergo a polymerization process, leaving a solid layer of the material. After that, more resin will be respreads on top of the printed layer, so that the laser can keep building up the desired final component. This technique is rather expensive because of the price of the photosensitive resin, but the final products printed with this method have a smooth surface finish.

Figure 1.1 shows a visual representation of SLA technology.^[38-41]

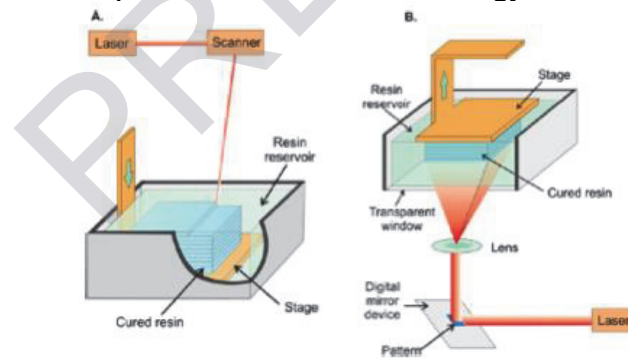


Figure 1.1 Two different stereolithography schematics. **a)** Bath stereolithography consists of a laser curing a layer of liquid resin. After one layer is cured, the stage lowers itself allowing for more liquid resin to cover the cured polymer. After that, laser cures the new layer of resin as specified by the design. **b)** This approach works in reverse process compared to the bath SLA. Here the stage is submerged inside the resin. Then, the stage is pulled up to allow more resin to flow below the cured polymer. A pattern can be added so that the laser can cure the whole layer design at the same time. Obtained from Ref[37]